THE JOURNAL OF PHYSICAL CHEMISTRY A

Article

Cite This: J. Phys. Chem. A 2018, 122, 6416−6423

pubs.acs.org/JPCA

Molecular Engineering toward Coexistence of Dielectric and Optical Switch Behavior in Hybrid Perovskite Phase Transition Material

Yuzhong Hu,[†] Hongbo Zhang,[†] Wee Kiang Chong,[†] Yongxin Li,[‡] Yujie Ke,[§] Rakesh Ganguly,[‡] Samuel Alexander Morris,[∥] Lu You,[§] Ting Yu,[†] Tze Chien Sum,[†] Yi Long,[§] and Hong Jin Fan*[,†,‡]

[†]School of Physical and Mathematical Sciences, Nanyang Technological University, Singapore 637371

[‡]Division of Chemistry and Biological Chemistry, School of Physical and Mathematical Sciences, Nanyang Technological University, 21 Nanyang Link, Singapore 637371

[§]School of Materials Science and Engineering, Nanyang Technological University, Singapore 639798

[∥]Facility for Analysis, Characterisation, Testing and Simulation (FACT), Nanyang Technological University, 50 Nanyang Avenue, Singapore 639798

ABSTRACT: Organic−inorganic hybrid perovskites with considerable dielectric differences near the phase transition are potential candidates as phase transition materials (PTMs). However, compared with traditional PTMs, which require multiple switchable channels, the hybrid perovskites so far show only switching behavior in dielectric constants. We herein report a new crystal design strategy and successful synthesis of a two-dimensional perovskite $(C_6H_5C_2H_4NH_3)_2MnCl_4$. In this hybrid perovskite, the manganese chloride octahedron is a crystal field sensitive luminescent molecular system. The distortion level of $MnCl_6^{4-}$ also depends on temperature during the order−disorder phase transition. Hence, such a manganese octahedron-based perovskite can exhibit switching behaviors in both dielectric and optical properties. We observe a 14% decrease in optical absorption and 1.6 times increase in dielectric constant during the phase transition at 365 K. In addition, the characteristic photoluminescence decreases by 17% in intensity. Such a molecule-based crystal design paves a new way to explore multifunctional PTMs based on organic−inorganic perovskites.

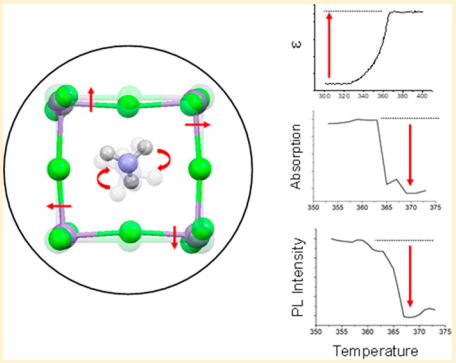

INTRODUCTION

Control and switch multiple physical channels such as optics and electrics are interesting topics because their special coupling effects such as optoelectronic and magnetoelectric may consequently lead to novel multifunctional devices.[1−4] The coexisting physical properties in a single phase make a multifunctional material capable of exploiting more than one task at the same time.[5−7] This special feature triggers a strong research impetus toward new design strategy and devices for multifunctional materials in various molecular systems.[2,8,9] With the flourishing development of hybrid perovskite solar cells, considerable research efforts have also been devoted to their luminescence, ferroelectricity, and crystal structure property.[10−12] The assembling of an organic, inorganic molecular network with each component carrying one functionality provides hybrid perovskite with intriguing promise as a multifunctional material.[13,14] For example, $(Me_3NCH_2C)MnCl_3$ reported by You et al. exhibits a large piezoelectric coefficient of 185 and strong photoluminescence (PL) at 640 nm.[15] The piezoelectric polarization comes from long-range-ordered dipoles consisting of $Me_3NCH_2C^+$ cations and $MnCl_6^{4-}$ anions, and the photoluminescence stems from the electron transition in the luminescence active manganese ion.

Phase transition materials (PTMs) is one of the intensively investigated topics in multifunctional materials where various physical channels, such as the dielectric constant (ε) and the absorption coefficient, show switchable behavior between considerably low and high states near the phase transition temperature. Materials with multiple switchable behaviors have high application potential in rewritable data storage, signal sensing, data communication, etc.[16−18] Great efforts have been made to trigger dielectric switch behavior and design multifunctional PTMs in several material systems, such as organics, hybrid perovskites, and metal−organic frameworks.[19−25] For example, Sun et al. realized a dielectric transition in an organic material by temperature-triggered molecular motion of the trifluoromethanesulfonate anionic moiety in 4-*N*,*N*-dimethylamino-4-*N*-methylstilbazolium trifluoromethanesulfonate.[20] Shi et al. reported two multifunctional phase transition materials based on hybrid perovskites, where both the dielectric constant and second harmonic generation exhibit low and high states around the phase transition temperature.[19] In these materials, the dielectric

Received: June 14, 2018
Revised: July 9, 2018
Published: July 16, 2018

DOI: 10.1021/acs.jpca.8b05693
J. Phys. Chem. A 2018, 122, 6416−6423

increases are attributed to the order−disorder transitions of organic cations, while the second harmonic generation switch behaviors are due to the transitions in the crystal's centrosymmetry property. However, in hybrid perovskites, though much progress has been made to design and synthesize new PTMs, most of them only exhibit dielectric switching behavior.[20,21,26,27] For their potential application in a conventional PTM field such as optical disk, different memory states manifested by low and high optical absorption are desirable.

In this work, we report a new design strategy and property of a hybrid perovskite $(C_6H_5C_2H_4NH_3)_2MnCl_4$ as a multifunctional PTM which exhibits coupled switch behaviors in dielectric, absorption, and PL. Here we first trace the design strategy of realizing absorption and PL switch behaviors in this material. In hybrid perovskite, optical properties such as PL are mainly determined by electron transition in the inorganic layer, so the length of the metal−halide chemical bond and structural distortion of the inorganic lattice play key roles in the optical absorption and emission.[28−30] Consequently, for the prospect of manipulating the optical property, one of the methods is to change the distortion level of the metal halide octahedron.[31−33] To this end, several methods have been reported, such as applying pressure,[34] employing different organic parts,[33] and triggering the phase transition.[31] Our strategy is to employ a metal halide octahedron which both has a crystal distortion sensitive optical property and goes through de-distortion molecular motion during phase transition. To design a molecular system with these two features, we consider a transition metal centered octahedral system. From crystal field theory, a transition metal centered octahedron system is a nonlinear one with degenerate energy states. This kind of system will spontaneously have Jahn−Teller distortion (JTD) to split its energy states and consequently remove its degeneracy.[35] In particular, with increasing temperature, the phase transition of MnX_6^{4-} (X, halide) octahedron based perovskites generally undergo a de-JTD process due to thermal effect.[35] Additionally, it is reported that $MnCl_6^{4-}$ exhibits high sensitivity of its optical absorption and PL to the crystal field strength, which changes with the distortion level.[36] Consequently, $(C_6H_5C_2H_4NH_3)_2MnCl_4$ is supposed to show both distortion sensitive optical properties and undergo de-JTD during phase transition. In addition, its large phenethylammonium (PEA) organic part leads to high stability and a two-dimensional (2D) structure feature, which is important for the miniaturization of memory material. Our measurements show that this crystal exhibits evident changes in optical absorption (13.7%) and PL intensity (17.5%) near the phase transition temperature. Another influence of de-JTD is the appearance of dielectric switch behavior at phase transition. With a decrease in distortion level, the symmetry of the inorganic layer becomes higher. This structure change induces equivalent energy states for the organic cation. At high temperatures, the PEA cations can overcome the energy barrier between equivalent states. As a result, order−disorder phase transition is triggered, accompanied by dielectric switch behavior.

RESULTS AND DISCUSSION

The crystal structures of $(PEA)_2MnCl_4$ single crystal were studied using X-ray single-crystal diffraction analysis at 300 K (room temperature phase, RTP) and 380 K (high temperature phase, HTP). Table 1 lists the basic crystal structure information. At RTP (Figure 1a), the crystal consists of $MnCl_6^{4-}$ inorganic layers and PEA organic layers. The metal halide octahedra share corners and form the 2D network, while PEA cations occupy the space enclosed by inorganic layers and link $MnCl_6^{4-}$ by hydrogen bonds between H in ammonias and Cl in metal halide octahedra. Different layers of perovskite are weakly bonded to each other by van der Waals interaction, making this material capable of being exfoliated to a nanometer level thin film. Within the metal halide layer, each manganese atom is surrounded by six chloride atoms, where four in-plane Cl atoms bridge Mn atoms in four nearby $MnCl_6^{4-}$ octahedra. Because of JTD, the inorganic layers show a distinct tilt both inside and between each metal halide octahedron. The Cl−Mn−Cl angles around Mn range from 88.68 to 91.32°, and the bridging angle (Mn−Cl−Mn) between octahedra is 168.56° (see Figure 1c).

Table 1. Crystallography Data of $(PEA)_2MnCl_4$ Measured at Two Different Temperatures

	RTP	HTP
empirical formula	$(C_6H_5C_2H_4NH_3)_2MnCl_4$	$(C_6H_5C_2H_4NH_3)_2MnCl_4$
formula weight	441.11	441.11
crystal system	orthorhombic	tetragonal
space group	*Pbca*	$I\bar{4}$
measurement temp (K)	300	380
a (Å)	7.159(3)	5.1435(3)
b (Å)	7.256(3)	5.1435(3)
c (Å)	39.280(15)	39.822(2)
lattice volume (Å^3)	2040.4(13)	1053.51(14)
absorption correction (mm^{-1})	1.170	1.133
Z	4	2
F(000)	908	454
T_{min}/T_{max}	0.9330/0.7060	0.9350/0.7130
goodness of fit (GOF)	1.074	1.124
R_1 [$I > 2\sigma(I)$]	0.0494	0.0425
wR_2 [$I > 2\sigma(I)$]	0.1229	0.1337

In the heating process, a phase transition toward higher disorder level of organic cation and de-JTD of metal halide octahedron occurs.[35] The crystal system changes from orthorhombic to tetrahedral structure, while the space group transfers from *Pbca* to $I\bar{4}$. At HTP (Figure 1b), the in-plane Cl−Mn−Cl angles change to 90° and out-of-plane angles range from 89.55 to 90.45°, which means the $MnCl_6^{4-}$ systems have almost become standard octahedra. The Mn−Cl−Mn bridging angle changes to 179.10° (Figure 1d), indicating that the distortion between adjacent metal halide octahedra has diminished. Because of the inorganic framework transition and thermal effect, the phenethylammonium cations exhibit a distinct disorder phase with all atoms apparently existing in two possible positions.

Differential scanning calorimetry (DSC) measurement is a powerful method for detecting reversible phase transition triggered by temperature (T_C). As shown in Figure 2a, there is an exothermal peak at 365 K and 2 K thermal hysteresis (the dip in the heating process and peak in the cooling process). The area under the phase transition curves yields values for an entropy change (ΔS) of 1.22 J/mol·K. From the Boltzmann equation, ΔS is given by $\Delta S = R \ln N$, where R is the gas constant and N is the number of sites in a disorder system. For a pure order−disorder phase transition, N is supposed to be 2

DOI: 10.1021/acs.jpca.8b05693
J. Phys. Chem. A 2018, 122, 6416−6423

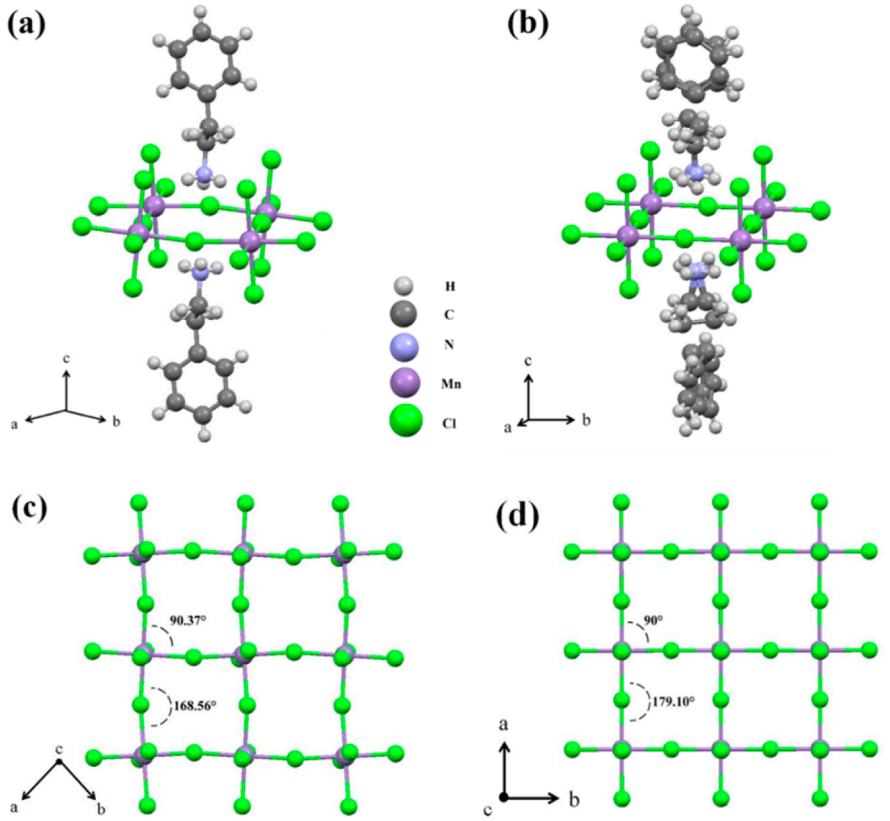

Figure 1. Comparison of crystal structures between RTP and HTP of $(PEA)_2MnCl_4$. Perspective views at 300 (a) and 380 K (b). Top views of inorganic layer at 300 (c) and 380 K (d).

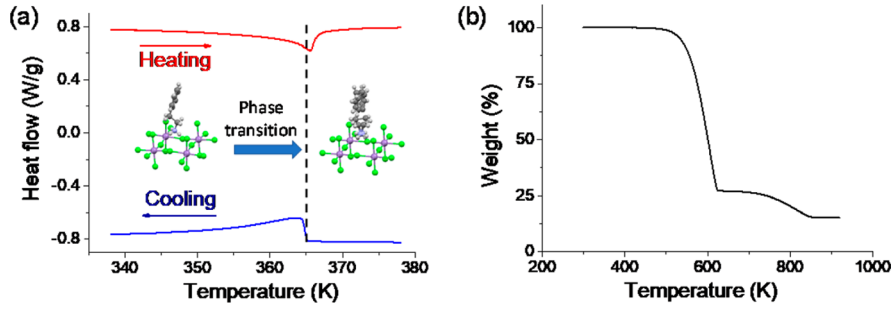

Figure 2. DSC curve obtained in a heating−cooling cycle (a) and TGA analysis (b) of the single crystal $(PEA)_2MnCl_4$.

or a larger integer.[37] The calculated N value for $(PEA)_2MnCl_4$ is 1.15, which indicates the phase transition near T_C = 365 K is a more complex one rather than the typical order−disorder type.[19,38] In addition, to investigate the thermostability, thermogravimetric analysis (TGA) was conducted on the bulk single crystal in air. The TGA curve reveals that $(PEA)_2MnCl_4$ is stable up to around 473 K (Figure 2b) and thus suggests this perovskite can meet the general working condition of an optoelectronic device.

Raman spectroscopy is a powerful method for the investigation of phase transition in layered materials.[39−41] In general, low-frequency Raman modes are often coupled to the order parameters of a phase transition.[42,43] In the Raman spectra recorded from our single crystal, two low-frequency modes are observed and both show an obvious temperature dependence (see Figure 3). At room temperature, these two modes are centered at 16 and 39 cm^{-1} (refer to α and β, respectively). The previous Raman study of PEA-type perovskites[44] reveals the α mode represents the shear mode of the organic layer with respect to the metal halide layer along the in-plane direction (see inset of Figure 3) while the β mode corresponds to the rotation of NH_3^+ along the c-axis. The intensities of α and β modes continue to decrease to T_C = 363 K, around which both peaks disappear. This phenomenon suggests a translational symmetry breaking. For a pure order−disorder phase transition, the soft mode energy does not go to zero at T_C.[44] But in this material, both α and β modes disappear around 363 K. This also indicates that the phase transition in $(PEA)_2MnCl_4$ is not a pure order−disorder type. Additionally, with temperature increasing close to T_C, both modes soften and broaden considerably. This behavior suggests the phase transition has a displacive nature, which is manifested by softening of collective excitation.[45−47] Hence, with an obvious order−disorder transition of the organic part in crystallographic measurement and significant dielectric switch behavior (to be discussed later), we conclude that the

DOI: 10.1021/acs.jpca.8b05693
J. Phys. Chem. A 2018, 122, 6416−6423

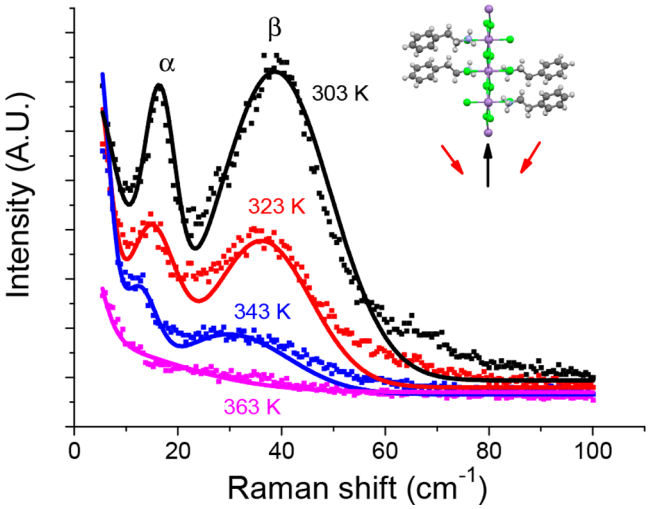

Figure 3. Temperature dependent Raman spectra of the $(PEA)_2MnCl_4$ crystal. The solid lines are fitted spectra. The inset shows the displacement direction of the α peak, where the red and black arrows indicate the inorganic and organic displacement directions, respectively.

phase transition at 363 K is an order−disorder type in conjunction with displacive nature appearing consistent with the DSC measurement.

It is found that several switchable properties coexist in our $(PEA)_2MnCl_4$ crystal around the phase transition temperature. We first discuss the dielectric constant. Here, measurement of the temperature dependent dielectric constant was performed on the bulk single crystal sample of $(PEA)_2MnCl_4$ in the heating mode. The well-defined facets indicate good quality of the bulk crystal (see Figure 4a). A pole figure was measured to confirm the direction of [100] and [010] of the HTP single crystal (Figure 4b). As shown in Figure 4c,d, steplike anomalies around 366 K can be observed along the [100] and [010] directions whereas no anomaly was found in the [001] direction. With the temperature approaching T_C, the dielectric constant increases by 1.64 and 1.66 times along the [100] and [010] directions, respectively.

The ε increase along the [100] and [010] directions and the anisotropy of the dielectric constant can be explained by the structure transformation during phase transition. As illustrated in Figure 5a, at RTP, the metal halide octahedron system has a relatively lower symmetry. With hydrogen bond interaction between PEA cations and inorganic octahedron systems, the organic cations will be fixed at a certain position where they have the lowest energy.[48] At HTP (Figure 5b), JTD has been almost eliminated, leading to expansion of the inorganic framework. As a result, the H−Cl hydrogen bonds are weakened due to the increased bonding length (from 2.40 to 2.69 Å at RTP and from 2.68 to 2.79 Å at HTP). Subsequently the degree of freedom of the cation increases and thus contributes to the switching behavior of the dielectric constant at HTP. More importantly, the de-JTD induces a mirror symmetry along the Mn−Cl−Mn bridges in each quasi-cuboid inorganic unit (see Figure 5b). Consequently, for the organic PEA cation, there are equivalent states with same energy in the diagonal plane of this quasi-cuboid system, which induces two possible positions and results in the order−disorder transition of the PEA cation. Therefore, with this temperature-induced change in crystal dynamics and higher degree of freedom, the organic cations are capable of switching between two equivalent states with a small energy barrier along the diagonal plane under ac electric field. Consequently, there is a linear relationship between the increases in permittivity along the [100] and [010] directions at T_C, which also explains why the corresponding dielectric constants increase by similar times (1.64 and 1.66).

As expected, the $(PEA)_2MnCl_4$ crystal is also an optical material. The absorption and PL spectra are illustrated in

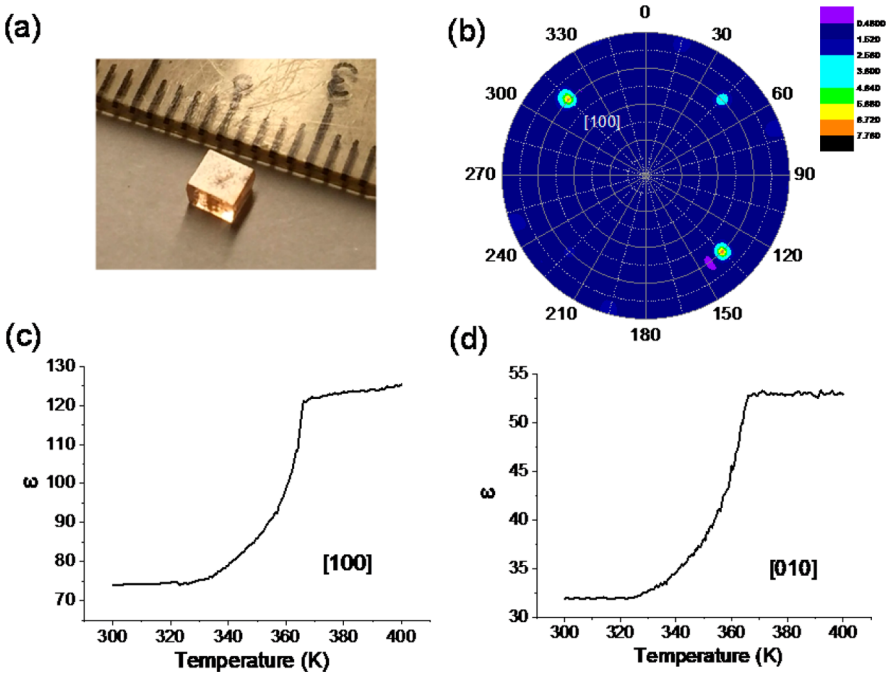

Figure 4. Photograph (a) and dielectric switch measurement of $(PEA)_2MnCl_4$. (b) Pole figure of bulk crystal. (c and d) Temperature dependent dielectric constant (ε) along the two crystallographic directions of [100] and [010] at 1 MHz ac electric field, respectively.

DOI: 10.1021/acs.jpca.8b05693
J. Phys. Chem. A 2018, 122, 6416−6423

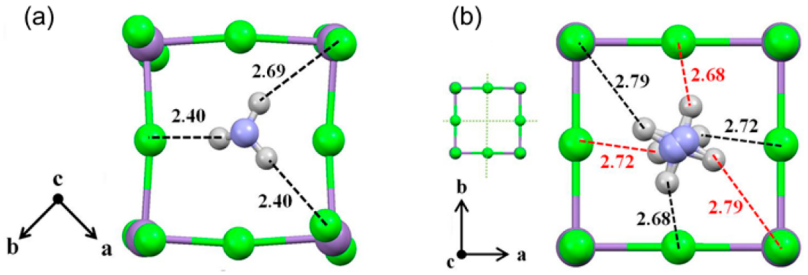

Figure 5. Crystal structure and length of hydrogen bonds (black and red dashed lines denote two different equivalent states. Length unit is angstroms at RTP (a) and HTP (b). Left middle of (b) is the symmetry property of inorganic system.

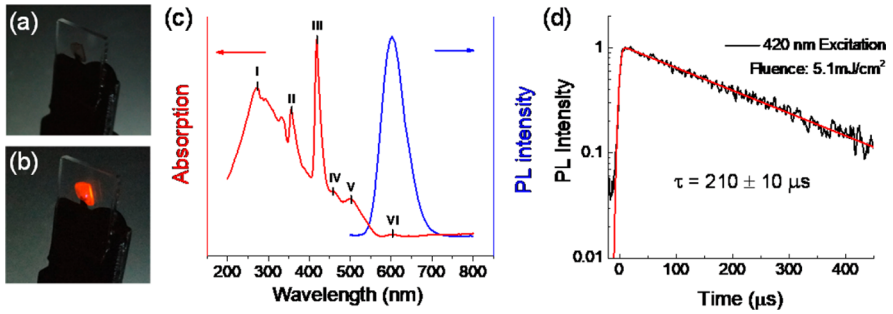

Figure 6. Photographs of bulk crystal (attached to a quartz substrate) (a) and luminescence under 420 nm excitation (b). Normalized absorption and photoluminescence spectra (c) and PL lifetime (d).

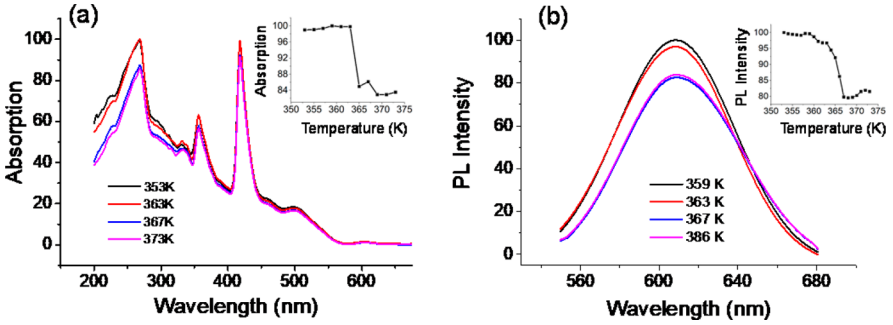

Figure 7. Normalized absorption (a) and PL spectra excited by 532 nm laser (b) near the phase transition temperature (365 K). The insets in (a) and (b) show the intensity change of the absorption at 265 nm and emission at 608 nm as a function of temperature, respectively.

Figure 6c. Six absorption peaks can be distinguished around 272, 356, 417, 458, 503, and 605 nm. Among them, peaks II–V are highly consistent with previous studies on the band structure of Mn^{2+}.[49] The weak absorption at 603 nm possibly originates from the direct electron transfer from the ground state to the first excited triplet state in Mn^{2+}.[50,51] Though the direct promotion of electron from ground state to triplet state is theoretically forbidden by the absorption selection rule, this transition may take place because of distortion or impurity in the crystal. Another peak at 272 nm stems from the transition between p orbitals of carbon and chlorine in the phenethylammonium cation.[52] In addition, our $(PEA)_2MnCl_4$ crystal is found to be strongly luminescent. Figure 6a is the photograph of the bulk crystal attached to a quartz. A strong orange-colored luminescence can be observed under 420 nm excitation (see Figure 6b), and the corresponding PL spectrum is shown in Figure 6c, where a broad emission peak is centered at 602 nm. The corresponding lifetime measurement of this 602 nm emission is shown in Figure 6d. The relatively large lifetime, 210 μs, lies in the general lifetime range of phosphorescence. Considering the relatively long PL lifetime, emission peak position, and luminescence metal ion origin, we can assign this orange phosphorescence to the $(t_{2g})^4(e_g)^1 \rightarrow (t_{2g})^3(e_g)^2$ transition in the octahedrally coordinated manganese.[3,50,51]

In addition to the aforementioned dielectric switch behavior, the change in optical property associated with the phase transition is an interesting topic in PTM.[16,19] Especially, much attention has been paid to the short wavelength and ultraviolet region since a laser beam with shorter wavelength can be focused to a smaller spot and achieve higher memory capacity.[16] To investigate possible optical switch behavior of our $(PEA)_2MnCl_4$ single crystal, we measured the absorption and PL spectra around the phase transition temperature (365 K). As demonstrated in Figure 7a, the absorption intensity shows 12.4 and 13.7% changes for the two peaks at 356 and 264 nm, respectively. The intensity differences before the onset of phase transition (between 353 and 363 K) and after T_C (between 367 and 373 K) of these two peaks are very small. Therefore, we can infer that this abrupt change in optical absorption across T_C results from the structure change rather than temperature difference. The absorption switching

DOI: 10.1021/acs.jpca.8b05693
J. Phys. Chem. A 2018, 122, 6416–6423

behavior at 265 nm may come from the disordered molecular motion of the PEA organic cation, while the change at 356 nm may be attributed to the change in the density of state triggered by different distortion levels in the metal halide octahedron.[34,53,54] The photoluminescence peak obtained by 532 nm excitation also shows a 17.5% intensity decrease with a slight red shift of 2 nm near the phase transition temperature (see Figure 7b). This intensity decrease may be attributed to the amorphous-order phase transition of the metal halide octahedron.[34,36,54] It may also be attracted to the shift of the excitation spectrum caused by removal of distortion in the $MnCl_6^{4-}$ system. The slight red shift comes from the changed axial crystal field, which is consistent with the previous report.[36]

In conclusion, by a molecular design strategy, we have successfully achieved the synthesis a 2D hybrid perovskite single crystal and demonstrated it to be a multifunctional phase transition material. The crystal exhibits coupled switching response in both the dielectric constant and optical absorption, as well as photoluminescence intensity near the phase transition point. The absorption and photoluminescence changes are induced by de-Jahn–Teller phase transition in the Mn-based octahedral system, which has a distortion sensitive absorption spectrum and PL spectrum. Dielectric switch behavior is induced by a coupled effect between order–disorder transition and inorganic layer symmetry change. This material design strategy may open a new avenue for the preparation of multifunctional phase transition materials based on organic–inorganic hybrid perovskites.

METHODS

Synthesis of $(PEA)_2MnCl_4$ Single Crystal. All chemicals were purchased from Sigma-Aldrich and used as received. Single crystal of $(PEA)_2MnCl_4$ was synthesized by reaction of 4 mmol of PEAHCl and 2 mmol of $MnCl_2$ at room temperature. Brown crystals with a nearly square face (Figure 4a) were obtained by slow evaporation of 4.4 mL of mixed methanol and deionized water with volume ration of 10:1.

X-ray Diffraction (XRD). The pole figure of the obtained crystal was measured on bulk single crystal. The XRD data were recorded by a Bruker D8 Discover thin film X-ray diffractometer (λ = 0.710 73 Å). Crystallographic data with approximate dimensions of 0.060 × 0.220 × 0.320 mm were collected using a Bruker APEX II diffractometer. The crystals of $(PEA)_2MnCl_4$ were measured at 300 and 380 K. The structure was solved by Bruker SHELXTL Software Package and refined for all data by full-matrix least squares on F^2. All non-hydrogen atoms were subjected to anisotropic refinement. The hydrogen atoms were generated geometrically and allowed to ride in their respective parent atoms; they were assigned appropriate isotropic thermal parameters and included in the structure factor calculations. The data can be obtained free of charge from The Cambridge Crystallographic Data Centre via www.ccdc.cam.ac.uk/data_request/cif.

Differential Scanning Calorimetry (DSC) Measurement. DSC was performed on a TA Q10 by heating and cooling the single crystal sample at a rate of 3 K min^{-1} in an aluminum pan under nitrogen at atmospheric pressure.

Thermogravimetric Analysis. Thermal stability was measured on bulk single crystal by a TGA/Q500 V6.7 Build 203 instrument at a rate of 10 K min^{-1} in air.

Dielectric Property. Dielectric measurement was carried out on a single crystal specimen by Agilent E 4980A with 1 V ac voltage and a conductive tip on the probe station. To measure in-plane dielectric property, interdigitated electrodes were deposited by evaporating 5 nm of chromium and 50 nm of gold on the bulk single crystal with a mask.

Absorption and PL Property. The absorption spectrum was recorded using an Agilent Technologies UV–vis–NIR spectrometer with a Cary 5000 model. The room temperature PL spectrum was measured by a Shimadzu RF 5301-PC spectrofluorophotometer. The temperature dependent PL spectrum was performed in a vacuum on a WITec Alpha300 Series confocal Raman system with a 600 g/mm grating and a 532 nm excitation laser. The temperature was controlled by a stage HFS600E from Linkam Scientific Instruments. Time-resolved PL measurements were conducted using 420 nm femtosecond excitation pulses (50 fs, 1 kHz). The back-scattered PL emission was collected and dispersed using a 150 g mm^{-1} spectrometer (Princeton Instruments), and temporally resolved using an Optronis streak camera system. The crystal lifetime (210 ± 10 μs) was determined by averaging lifetimes from three different crystal positions. All these measurements were conducted on bulk single crystal.

Raman Spectrum. Raman spectra were recorded using a WITec Alpha300 Series confocal Raman system in a vacuum with a 2400 lines mm^{-1} grating and a 50× objective under 532 nm laser excitation. The laser power was kept at 1 mW. All the Raman and PL temperature dependent measurements were conducted in a vacuum chamber, and the temperature was controlled by a stage HFS600E from Linkam Scientific Instruments.

AUTHOR INFORMATION

Corresponding Author

*E-mail: fanhj@ntu.edu.sg.

ORCID

Tze Chien Sum: 0000-0003-4049-2719

Yi Long: 0000-0003-0608-8253

Hong Jin Fan: 0000-0003-1237-4555

Notes

The authors declare no competing financial interest.

ACKNOWLEDGMENTS

This work is supported by Singapore MOE AcRF Tier 1 grants (RG115/15 and RG199/17) and a MOE Tier 2 grant (MOE2015-T2-2-015).

REFERENCES

(1) Wen, Z.; Li, C.; Wu, D.; Li, A.; Ming, N. Ferroelectric-Field-Effect-Enhanced Electroresistance in Metal/Ferroelectric/Semiconductor Tunnel Junctions. *Nat. Mater.* **2013**, *12*, 617–621.

(2) Hao, J.; Zhang, Y.; Wei, X. Electric-Induced Enhancement and Modulation of Upconversion Photoluminescence in Epitaxial Batio3:Yb/Er Thin Films. *Angew. Chem.* **2011**, *123*, 7008–7012.

(3) Ye, H. Y.; Zhou, Q.; Niu, X.; Liao, W. Q.; Fu, D. W.; Zhang, Y.; You, Y. M.; Wang, J.; Chen, Z. N.; Xiong, R. G. High-Temperature Ferroelectricity and Photoluminescence in a Hybrid Organic-Inorganic Compound: (3-Pyrrolinium)Mncl3. *J. Am. Chem. Soc.* **2015**, *137*, 13148–54.

(4) Yao, Q.; Wang, F.; Xu, F.; Leung, C. M.; Wang, T.; Tang, Y.; Ye, X.; Xie, Y.; Sun, D.; Shi, W. Electric Field-Induced Giant Strain and Photoluminescence-Enhancement Effect in Rare-Earth Modified Lead-Free Piezoelectric Ceramics. *ACS Appl. Mater. Interfaces* **2015**, *7*, 5066–5075.

DOI: 10.1021/acs.jpca.8b05693
J. Phys. Chem. A 2018, 122, 6416–6423

(5) Itkis, M.; Chi, X.; Cordes, A.; Haddon, R. Magneto-Opto-Electronic Bistability in a Phenalenyl-Based Neutral Radical. *Science* **2002**, *296*, 1443−1445.
(6) Kahn, O.; Martinez, C. J. Spin-Transition Polymers: From Molecular Materials toward Memory Devices. *Science* **1998**, *279*, 44−48.
(7) Gaultois, M. W.; Barton, P. T.; Birkel, C. S.; Misch, L. M.; Rodriguez, E. E.; Stucky, G. D.; Seshadri, R. Structural Disorder, Magnetism, and Electrical and Thermoelectric Properties of Pyrochlore Nd2ru2o7. *J. Phys.: Condens. Matter* **2013**, *25*, 186004.
(8) Zhang, Y.; Liao, W. Q.; Fu, D. W.; Ye, H. Y.; Chen, Z. N.; Xiong, R. G. Highly Efficient Red-Light Emission in an Organic-Inorganic Hybrid Ferroelectric: (Pyrrolidinium)Mncl(3). *J. Am. Chem. Soc.* **2015**, *137*, 4928−31.
(9) Melot, B. C.; Goldman, A.; Darago, L. E.; Furman, J. D.; Rodriguez, E. E.; Seshadri, R. Magnetic Ordering and Magnetodielectric Phenomena in Coseo4. *J. Phys.: Condens. Matter* **2010**, *22*, 506003.
(10) Shi, Z.; Guo, J.; Chen, Y.; Li, Q.; Pan, Y.; Zhang, H.; Xia, Y.; Huang, W. Lead-Free Organic−Inorganic Hybrid Perovskites for Photovoltaic Applications: Recent Advances and Perspectives. *Adv. Mater.* **2017**, *29*, 1605005.
(11) Hu, T.; Smith, M. D.; Dohner, E. R.; Sher, M.-J.; Wu, X.; Trinh, M. T.; Fisher, A.; Corbett, J.; Zhu, X.-Y.; Karunadasa, H. I.; Lindenberg, A. M. Mechanism for Broadband White-Light Emission from Two-Dimensional (110) Hybrid Perovskites. *J. Phys. Chem. Lett.* **2016**, *7*, 2258−2263.
(12) Liao, W. Q.; Zhang, Y.; Hu, C. L.; Mao, J. G.; Ye, H. Y.; Li, P. F.; Huang, S. D.; Xiong, R. G. A Lead-Halide Perovskite Molecular Ferroelectric Semiconductor. *Nat. Commun.* **2015**, *6*, 7338.
(13) Zhang, Y.; Liao, W. Q.; Fu, D. W.; Ye, H. Y.; Liu, C. M.; Chen, Z. N.; Xiong, R. G. The First Organic-Inorganic Hybrid Luminescent Multiferroic: (Pyrrolidinium)Mnbr3. *Adv. Mater.* **2015**, *27*, 3942−6.
(14) Bellitto, C.; Bauer, E. M.; Righini, G. Organic−Inorganic Hybrids: From Magnetic Perovskite Metal (Ii) Halides to Multifunctional Metal (Ii) Phosphonates. *Coord. Chem. Rev.* **2015**, *289−290*, 123−136.
(15) You, Y. M.; Liao, W. Q.; Zhao, D.; Ye, H. Y.; Zhang, Y.; Zhou, Q.; Niu, X.; Wang, J.; Li, P.; Fu, D.; Wang, Z.; Gao, S.; Yang, K.; Liu, J.; Li, J.; Yan, Y.; Xiong, R. An Organic-Inorganic Perovskite Ferroelectric with Large Piezoelectric Response. *Science* **2017**, *357*, 306−309.
(16) Wuttig, M.; Yamada, N. Phase-Change Materials for Rewriteable Data Storage. *Nat. Mater.* **2007**, *6*, 824−832.
(17) Salinga, M.; Wuttig, M. Phase-Change Memories on a Diet. *Science* **2011**, *332*, 543−544.
(18) Sun, Z.; Luo, J.; Zhang, S.; Ji, C.; Zhou, L.; Li, S.; Deng, F.; Hong, M. Solid-State Reversible Quadratic Nonlinear Optical Molecular Switch with an Exceptionally Large Contrast. *Adv. Mater.* **2013**, *25*, 4159−4163.
(19) Shi, P.-P.; Ye, Q.; Li, Q.; Wang, H.-T.; Fu, D.-W.; Zhang, Y.; Xiong, R.-G. Novel Phase-Transition Materials Coupled with Switchable Dielectric, Magnetic, and Optical Properties:[(Ch3) 4p][Fecl4] and [(Ch3) 4p][Febr4]. *Chem. Mater.* **2014**, *26*, 6042−6049.
(20) Sun, Z.; Luo, J.; Chen, T.; Li, L.; Xiong, R. G.; Tong, M. L.; Hong, M. Distinct Molecular Motions in a Switchable Chromophore Dielectric 4-N, N-Dimethylamino-4′-N′-Methylstilbazolium Trifluoromethanesulfonate. *Adv. Funct. Mater.* **2012**, *22*, 4855−4861.
(21) Zhang, W.; Ye, H.-Y.; Graf, R.; Spiess, H. W.; Yao, Y.-F.; Zhu, R.-Q.; Xiong, R.-G. Tunable and Switchable Dielectric Constant in an Amphidynamic Crystal. *J. Am. Chem. Soc.* **2013**, *135*, 5230−5233.
(22) Tang, Y.-Z.; Wang, B.; Zhou, H.-T.; Chen, S.-P.; Tan, Y.-H.; Wang, C.-F.; Yang, C.-S.; Wen, H.-R. Reversible Phase Transition with Ultralarge Dielectric Relaxation Behaviors in Succinimide Lithium(I) Hybrids. *Inorg. Chem.* **2018**, *57*, 1196−1202.
(23) Sun, Z.; Zeb, A.; Liu, S.; Ji, C.; Khan, T.; Li, L.; Hong, M.; Luo, J. Exploring a Lead-Free Semiconducting Hybrid Ferroelectric with a Zero-Dimensional Perovskite-Like Structure. *Angew. Chem., Int. Ed.* **2016**, *55*, 11854−11858.
(24) Sun, Z.; Liu, X.; Khan, T.; Ji, C.; Asghar, M. A.; Zhao, S.; Li, L.; Hong, M.; Luo, J. A Photoferroelectric Perovskite-Type Organometallic Halide with Exceptional Anisotropy of Bulk Photovoltaic Effects. *Angew. Chem., Int. Ed.* **2016**, *55*, 6545−6550.
(25) Li, L.; Shang, X.; Wang, S.; Dong, N.; Ji, C.; Chen, X.; Zhao, S.; Wang, J.; Sun, Z.; Hong, M.; Luo, J. Bilayered Hybrid Perovskite Ferroelectric with Giant Two-Photon Absorption. *J. Am. Chem. Soc.* **2018**, *140*, 6806−6809.
(26) Shi, X.; Luo, J.; Sun, Z.; Li, S.; Ji, C.; Li, L.; Han, L.; Zhang, S.; Yuan, D.; Hong, M. Switchable Dielectric Phase Transition Induced by Ordering of Twisting Motion in 1, 4-Diazabicyclo [2.2. 2] Octane Chlorodifluoroacetate. *Cryst. Growth Des.* **2013**, *13*, 2081−2086.
(27) Ji, C.; Sun, Z.; Zhang, S.-Q.; Chen, T.; Zhou, P.; Tang, Y.; Zhao, S.; Luo, J. Switchable Dielectric Behaviour Associated with above Room-Temperature Phase Transition in N-Isopropylbenzylammonium Dichloroacetate (N-Ipbadc). *J. Mater. Chem. C* **2014**, *2*, 6134−6139.
(28) Chen, Q.; De Marco, N.; Yang, Y.; Song, T.-B.; Chen, C.-C.; Zhao, H.; Hong, Z.; Zhou, H.; Yang, Y. Under the Spotlight: The Organic−Inorganic Hybrid Halide Perovskite for Optoelectronic Applications. *Nano Today* **2015**, *10*, 355−396.
(29) Wang, T.; Daiber, B.; Frost, J. M.; Mann, S. A.; Garnett, E. C.; Walsh, A.; Ehrler, B. Indirect to Direct Bandgap Transition in Methylammonium Lead Halide Perovskite. *Energy Environ. Sci.* **2017**, *10*, 509−515.
(30) Stoumpos, C. C.; Frazer, L.; Clark, D. J.; Kim, Y. S.; Rhim, S. H.; Freeman, A. J.; Ketterson, J. B.; Jang, J. I.; Kanatzidis, M. G. Hybrid Germanium Iodide Perovskite Semiconductors: Active Lone Pairs, Structural Distortions, Direct and Indirect Energy Gaps, and Strong Nonlinear Optical Properties. *J. Am. Chem. Soc.* **2015**, *137*, 6804−6819.
(31) Quarti, C.; Mosconi, E.; Ball, J. M.; D'Innocenzo, V.; Tao, C.; Pathak, S.; Snaith, H. J.; Petrozza, A.; De Angelis, F. Structural and Optical Properties of Methylammonium Lead Iodide across the Tetragonal to Cubic Phase Transition: Implications for Perovskite Solar Cells. *Energy Environ. Sci.* **2016**, *9*, 155−163.
(32) Jaffe, A.; Lin, Y.; Karunadasa, H. I. Halide Perovskites under Pressure: Accessing New Properties through Lattice Compression. *ACS Energy. Lett.* **2017**, *2*, 1549−1555.
(33) Cortecchia, D.; Neutzner, S.; Srimath Kandada, A. R.; Mosconi, E.; Meggiolaro, D.; De Angelis, F.; Soci, C.; Petrozza, A. Broadband Emission in Two-Dimensional Hybrid Perovskites: The Role of Structural Deformation. *J. Am. Chem. Soc.* **2017**, *139*, 39−42.
(34) Wang, L.; Wang, K.; Zou, B. Pressure-Induced Structural and Optical Properties of Organometal Halide Perovskite-Based Formamidinium Lead Bromide. *J. Phys. Chem. Lett.* **2016**, *7*, 2556−2562.
(35) Depmeier, W.; Felsche, J.; Wildermuth, G. Phases and Phase Transitions of Compounds (Cnh2n+ 1nh3) 2mncl4 with N= 1, 2, 3. *J. Solid State Chem.* **1977**, *21*, 57−65.
(36) Nataf, L.; Rodríguez, F.; Valiente, R.; González, J. Spectroscopic and Luminescence Properties of (Ch 3) 4nmncl3: A Sensitive Mn 2+-Based Pressure Gauge. *High Pressure Res.* **2009**, *29*, 653−659.
(37) Jain, P.; Ramachandran, V.; Clark, R. J.; Zhou, H. D.; Toby, B. H.; Dalal, N. S.; Kroto, H. W.; Cheetham, A. K. Multiferroic Behavior Associated with an Order− Disorder Hydrogen Bonding Transition in Metal− Organic Frameworks (Mofs) with the Perovskite Abx3 Architecture. *J. Am. Chem. Soc.* **2009**, *131*, 13625−13627.
(38) Liu, Y.; Chen, Y.; Xu, M.-j.; Zhu, C.-L.; Liu, Z.-q. Synthesis, Structure, and Phase Transition of a Novel Proton Transfer in a Supramolecular Cation with 2-Nitroanilinium Based on 18-Crown-6. *J. Mol. Struct.* **2017**, *1148*, 429−434.
(39) Kang, Y.; Najmaei, S.; Liu, Z.; Bao, Y.; Wang, Y.; Zhu, X.; Halas, N. J.; Nordlander, P.; Ajayan, P. M.; Lou, J.; Fang, Z. Plasmonic Hot Electron Induced Structural Phase Transition in a MoS2 Monolayer. *Adv. Mater.* **2014**, *26*, 6467−6471.

DOI: 10.1021/acs.jpca.8b05693
J. Phys. Chem. A 2018, 122, 6416−6423

(40) Hagemann, H.; Bill, H. Raman Spectroscopic Study of Structural Phase Transitions in the Layer Crystals (Etnh3) 2mcl4 with M= Cd and Mn. *J. Phys. C: Solid State Phys.* **1985**, *18*, 6441.
(41) Zhang, X.; Qiao, X.-F.; Shi, W.; Wu, J.-B.; Jiang, D.-S.; Tan, P.-H. Phonon and Raman Scattering of Two-Dimensional Transition Metal Dichalcogenides from Monolayer, Multilayer to Bulk Material. *Chem. Soc. Rev.* **2015**, *44*, 2757−2785.
(42) Scott, J. Soft-Mode Spectroscopy: Experimental Studies of Structural Phase Transitions. *Rev. Mod. Phys.* **1974**, *46*, 83.
(43) Petzelt, J.; Dvorak, V. Changes of Infrared and Raman Spectra Induced by Structural Phase Transitions. I. General Considerations. *J. Phys. C: Solid State Phys.* **1976**, *9*, 1571.
(44) Caretta, A.; Miranti, R.; Havenith, R. W. A.; Rampi, E.; Donker, M. C.; Blake, G. R.; Montagnese, M.; Polyakov, A. O.; Broer, R.; Palstra, T. T. M.; van Loosdrecht, P. H. M. Low-Frequency Raman Study of the Ferroelectric Phase Transition in a Layered CuCl4-Based Organic-Inorganic Hybrid. *Phys. Rev. B: Condens. Matter Mater. Phys.* **2014**, *89*, 024301.
(45) Cochran, W. Crystal Stability and the Theory of Ferroelectricity. *Adv. Phys.* **1960**, *9*, 387−423.
(46) Schneider, T.; Srinivasan, G.; Enz, C. Phase Transitions and Soft Modes. *Phys. Rev. A: At., Mol., Opt. Phys.* **1972**, *5*, 1528.
(47) Lines, M. E.; Glass, A. M. *Principles and Applications of Ferroelectrics and Related Materials*; Oxford University Press: 1977.
(48) Mitzi, D. B. Templating and Structural Engineering in Organic−Inorganic Perovskites. *J. Chem. Soc., Dalton Trans.* **2001**, 1−12.
(49) Lawson, K. E. Optical Studies of Electronic Transitions in Hexa- and Tetracoordinated Mn2+ Crystals. *J. Chem. Phys.* **1967**, *47*, 3627−3633.
(50) Orgel, L. Band Widths in the Spectra of Manganous and Other Transition-Metal Complexes. *J. Chem. Phys.* **1955**, *23*, 1824−1826.
(51) Orgel, L. Phosphorescence of Solids Containing the Manganous or Ferric Ions. *J. Chem. Phys.* **1955**, *23*, 1958−1958.
(52) Kassou, S.; El-Mrabet, R.; Kaiba, A.; Guionneau, P.; Belaaraj, A. Combined Experimental and Density Functional Theory Studies of an Organic−Inorganic Hybrid Perovskite. *Phys. Chem. Chem. Phys.* **2016**, *18*, 9431−9436.
(53) Amat, A.; Mosconi, E.; Ronca, E.; Quarti, C.; Umari, P.; Nazeeruddin, M. K.; Grätzel, M.; De Angelis, F. Cation-Induced Band-Gap Tuning in Organohalide Perovskites: Interplay of Spin−Orbit Coupling and Octahedra Tilting. *Nano Lett.* **2014**, *14*, 3608−3616.
(54) Wang, Y.; Lü, X.; Yang, W.; Wen, T.; Yang, L.; Ren, X.; Wang, L.; Lin, Z.; Zhao, Y. Pressure-Induced Phase Transformation, Reversible Amorphization, and Anomalous Visible Light Response in Organolead Bromide Perovskite. *J. Am. Chem. Soc.* **2015**, *137*, 11144−11149.

DOI: 10.1021/acs.jpca.8b05693
J. Phys. Chem. A 2018, 122, 6416−6423